Supplementary Materials

Selection of healthy sperm based on positive rheotaxis using a microfluidic device

Sandhya Sharma[a,b], Md. Alamgir Kabir[a,b], and Waseem Asghar[a,b,c,*]

[a]Department of Electrical Engineering and Computer Science, Florida Atlantic University, Boca Raton, FL 33431, USA

[b]Asghar-Lab, Micro and Nanotechnology in Medicine, College of Engineering and Computer Science, Boca Raton, FL 33431, USA

[c]Department of Biological Sciences (Courtesy Appointment), Florida Atlantic University, Boca Raton, FL 33431, USA

* Corresponding Author: Waseem Asghar, Email: wasghar@fau.edu

Table of Contents

1. Supplementary Videos

Video S1 (A, B & C): Videos represent the sperm track used to analyze various velocities from stock, no-flow (control), and with-flow group.

Video S2 (A, B & C): Videos illustrating the extent of difficulty faced by sperm cells while entering channel "b" at 2 $\mu L/min$, 1 $\mu L/min$ and 0.5 $\mu L/min$ respectively.

Video S3 (A): Video representing 0.5 $\mu L/min$ is an optimal rate where the sperm cells were seen actively swimming against the flow in channel "b".

Video S3 (B): Video representing at 10.5 $\mu L/min$ induced high force in channel "b", due to which the sperm cells were unable to enter the channel "b" thereby avoiding contamination.

Video S4: Video showing sperm cells facing hindrance due to a high flow rate because of reduced width in channel "a".

Video S5: Videos illustrating no-flow conditions inside the chip after semen loading**.**

2. Supplementary Table

Supplementary Table 1: Comparison of the data obtained from the existing microfluidic sperm sorting chips in terms of motility, sperm DNA fragmentation (SDF), morphology analysis and recovery rate, along with their limitations.

Devices/Studies	Motility	SDF	Morphology analysis	Recovery rate	Limitations
With-flow (from this paper)	99.47± 0.62%	2.6±1.04 % (84% improvement)	61.56 ±1.93%	1.38 ± 0.97%	
No-flow (control) (from this paper)	81± 04%	3.9±0.33 % (74% improvement)	44.65± 2.41%	1.46 ± 1%	Dead and immotile sperm cells in the collected sample
[1]	100%		NA	NA	Inconvenient sample collection with flow on and off process.
[2]	NA	NA	NA	NA	Sorted sperm sample was not collected
[3]	99.46 (± 0.92)	6 ± 0.45%	48%	28%	
[4]	NA	NA	NA	NA	Sorted sperm sample was not collected
[5]	NA	NA	NA	NA	Sorted sperm sample was not collected
[6]	100%	NA	NA	1.94 ± 0.32%	1) Sorted sperm sample was not collected 2) Cell entrapment for a brief time frame
[7]	82.9 ±15.06%	NA	NA	18.26 ±10.31%	Non-motile and dead cells in the collected sample

8	NA	NA	NA	NA	Sorted sperm sample was not collected
9	The standard deviation between inlet and collection chamber is ±7%	NA	NA	NA	1) Flow turned off and then reversed to direct the cells towards collecting chamber. 2) Sample is collected using CryoTip 3) Only 5 sperm cells are trapped at one time
10	32.58%	NA	NA	NA	1) Require multiple equipments for the device function. 2) Non-motile sperm cells in the collected sample
11	82.24%	NA	NA	NA	Sorted sperm sample was not collected
12	NA	NA	NA	NA	Sorted sperm sample was not collected

[13]	70.9 ± 4.5 %	NA	77.5 ± 6.4%	NA	The collected sample contained some non-viable cells
[14]	90%	NA	NA	NA	Sorted sperm sample was not collected
[15]	93%	NA	NA	NA	Low motility or dead sperm cells in the outlet.
[16]	Motility index 148, 15 & 0	NA	NA	NA	1) Use of resistive pulse measurement is is necessary for the small aperture 2) The aperture gets clogged due to debris from the reservoir
[17]	95.4 ± 3 %	0.8 ± 1.9 %	NA	3.6 ± 4 %	Preprocessing of the semen sample is required using 20 μm pore size filter before loading onto the chip.
[18]	<90%	3-6%	~56%	NA	Complicated chip assembly
[19]	NA	NA	NA	80% improvement	Complicated chip assembly
[20]	95.7%	NA	NA	NA	Lose some good-quality sperm cells.
[21]	93.6±1.6 % viability	1.63±0.79	NA	NA	The collected sample contained some non-viable cells

3. Microfluidic chip image

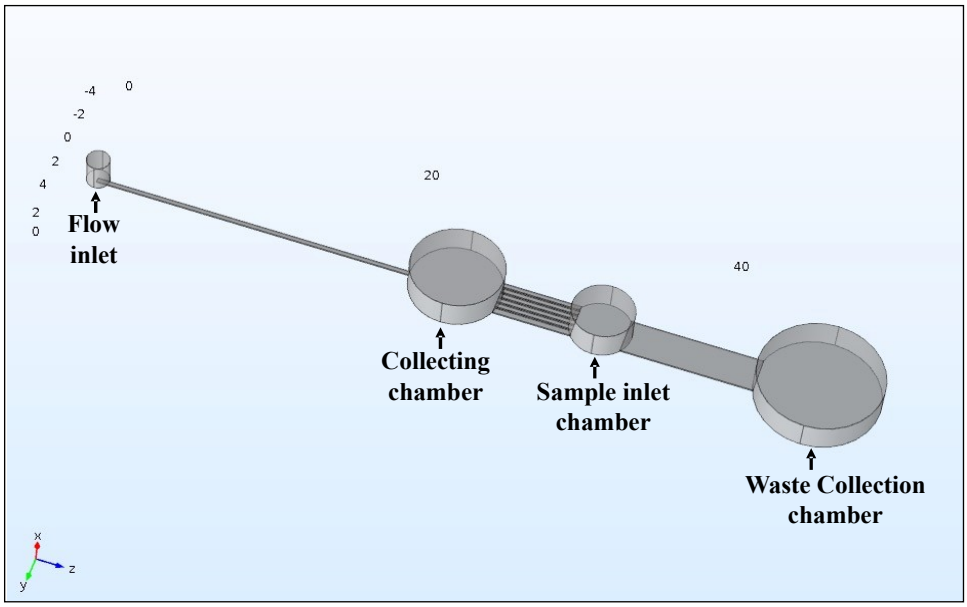

Fig. S1: The 3D image of the microfluidic chip designed in COMSOL

4. Morphology assessment images

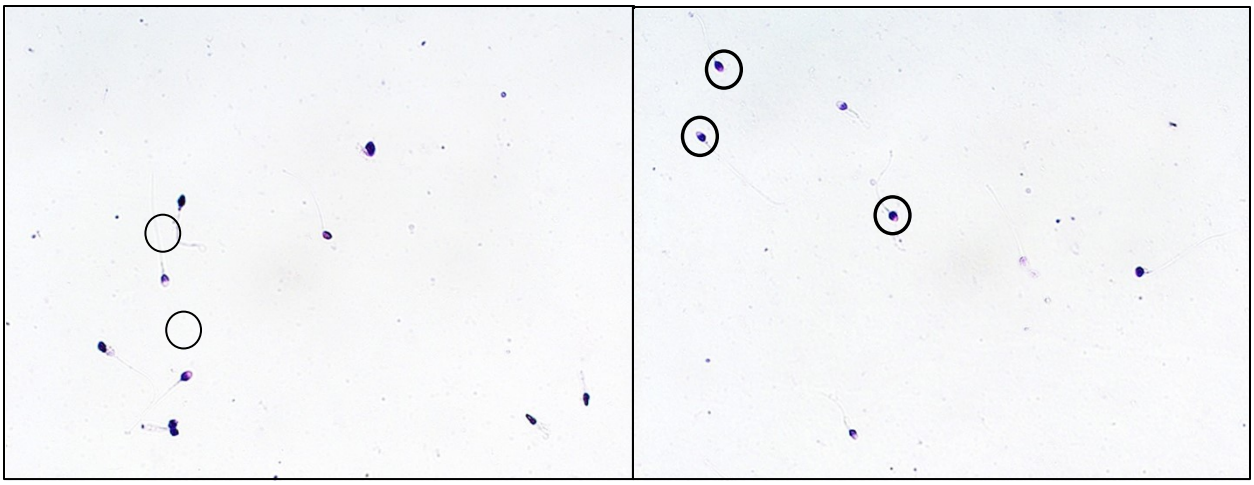

Fig. S2 (A): Brightfield images of the sperm cells (from stock) obtained with 40X objective. The sperm cells encircled with black are morphologically normal, and others are morphologically abnormal with principal piece coiled, pyriform head, tapered head, small tail or bent neck.

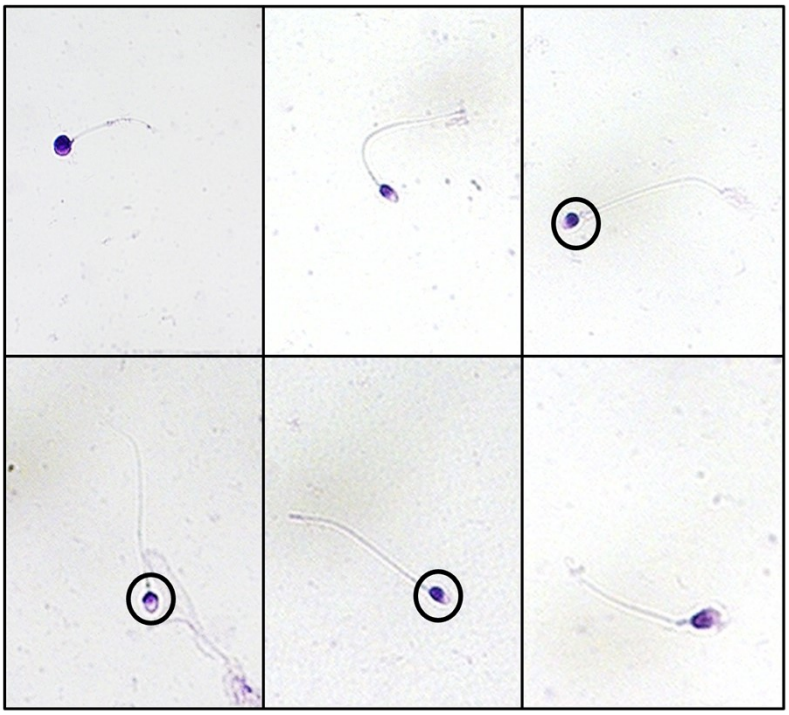

Fig. S2 (B): 40X objective brightfield images of the sperm cells isolated from the collection chamber of the chip with the no-flow (control) condition. The sperm cells encircled with black are morphologically normal, and others are morphologically abnormal with principal piece coiled, pyriform head, tapered head, small tail or bent neck.

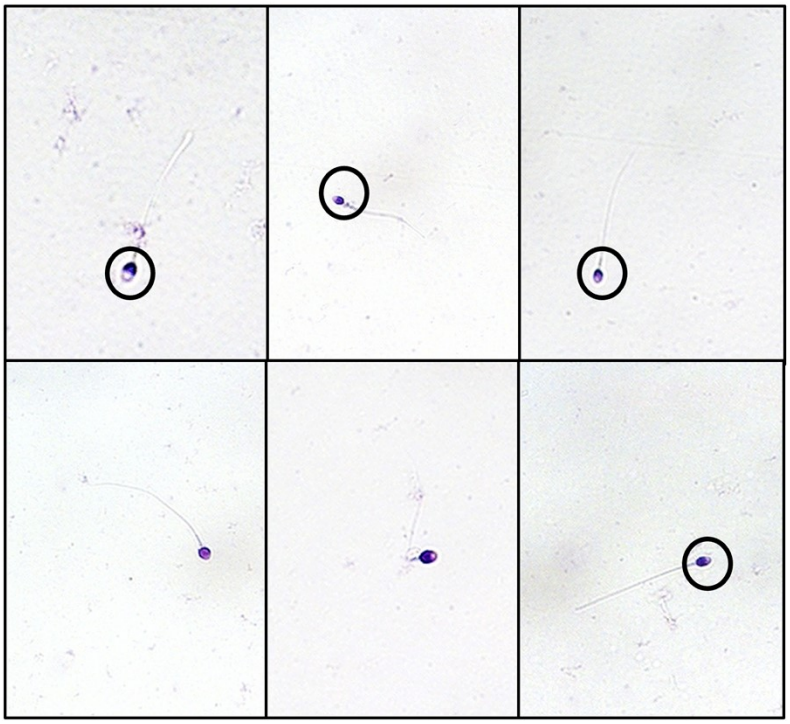

Fig. S2 (C): 40X objective brightfield images of the sperm cells isolated from the collection chamber of the chip with-flow (0.5 $\mu l/min$ rate) conditions. The sperm cells encircled with black are morphologically normal, and others are morphologically abnormal with principal piece coiled, pyriform head, tapered head, small tail or bent neck.

5. DNA fragmentation assessment images

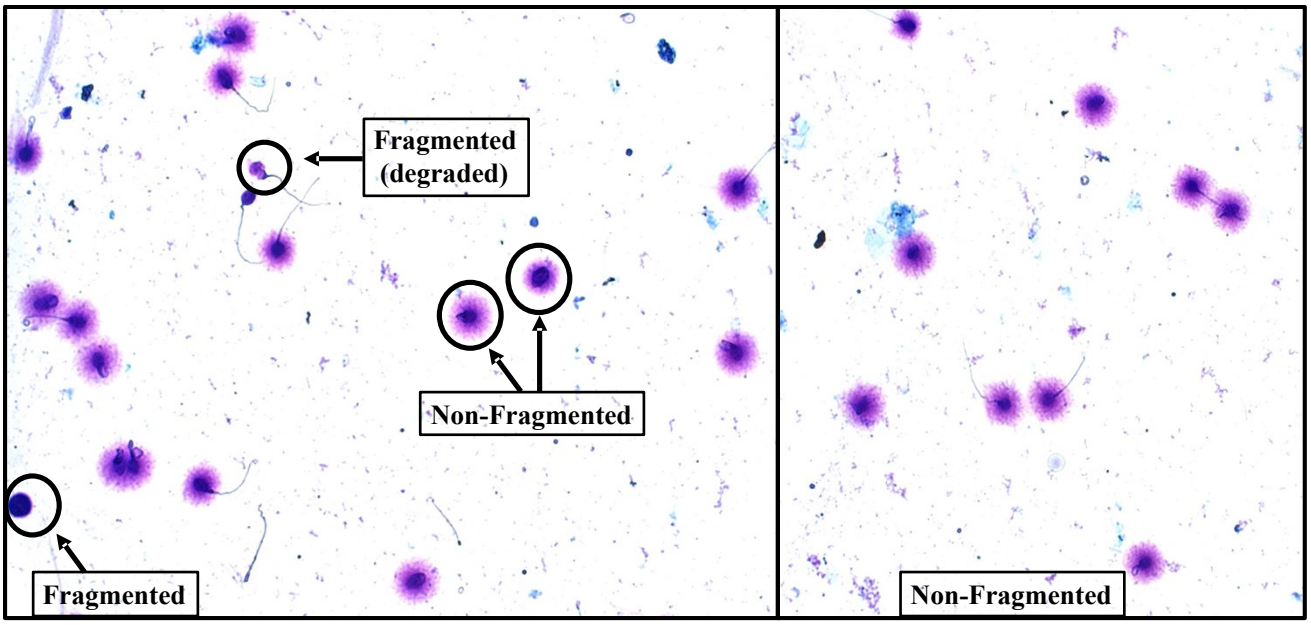

Fig. S3 (A): Brightfield images of the sperm cells (from stock) obtained with 40X objective. Sperm cells showing big and medium halo have non-fragmented DNA. Sperm cells showing no halo have fragmented DNA.

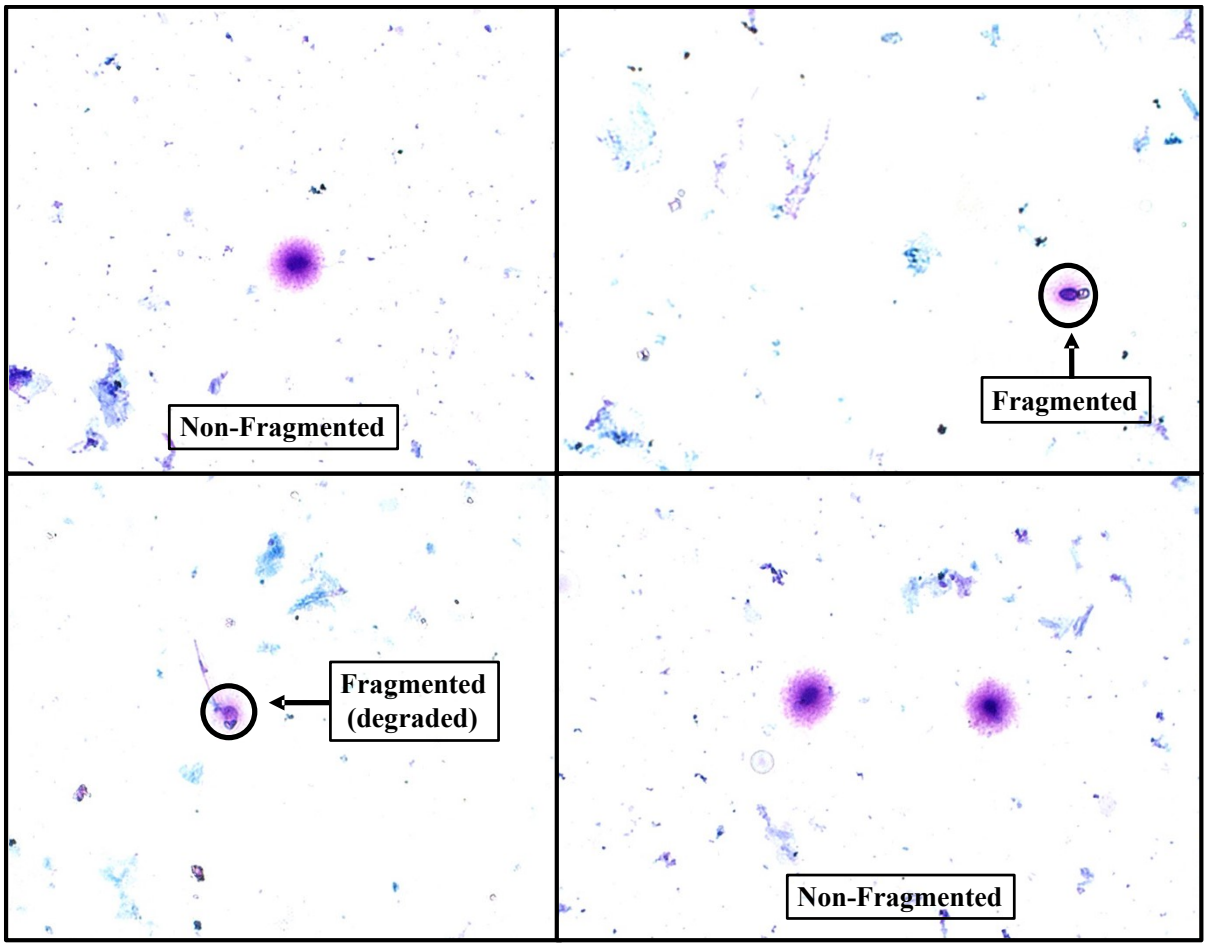

Fig. S3 (B): 40X objective brightfield images of the sperm cells isolated from the collection chamber of the chip with no-flow (control) condition. Sperm cells showing big and medium halo have non-fragmented DNA. Sperm cells showing no halo have fragmented DNA.

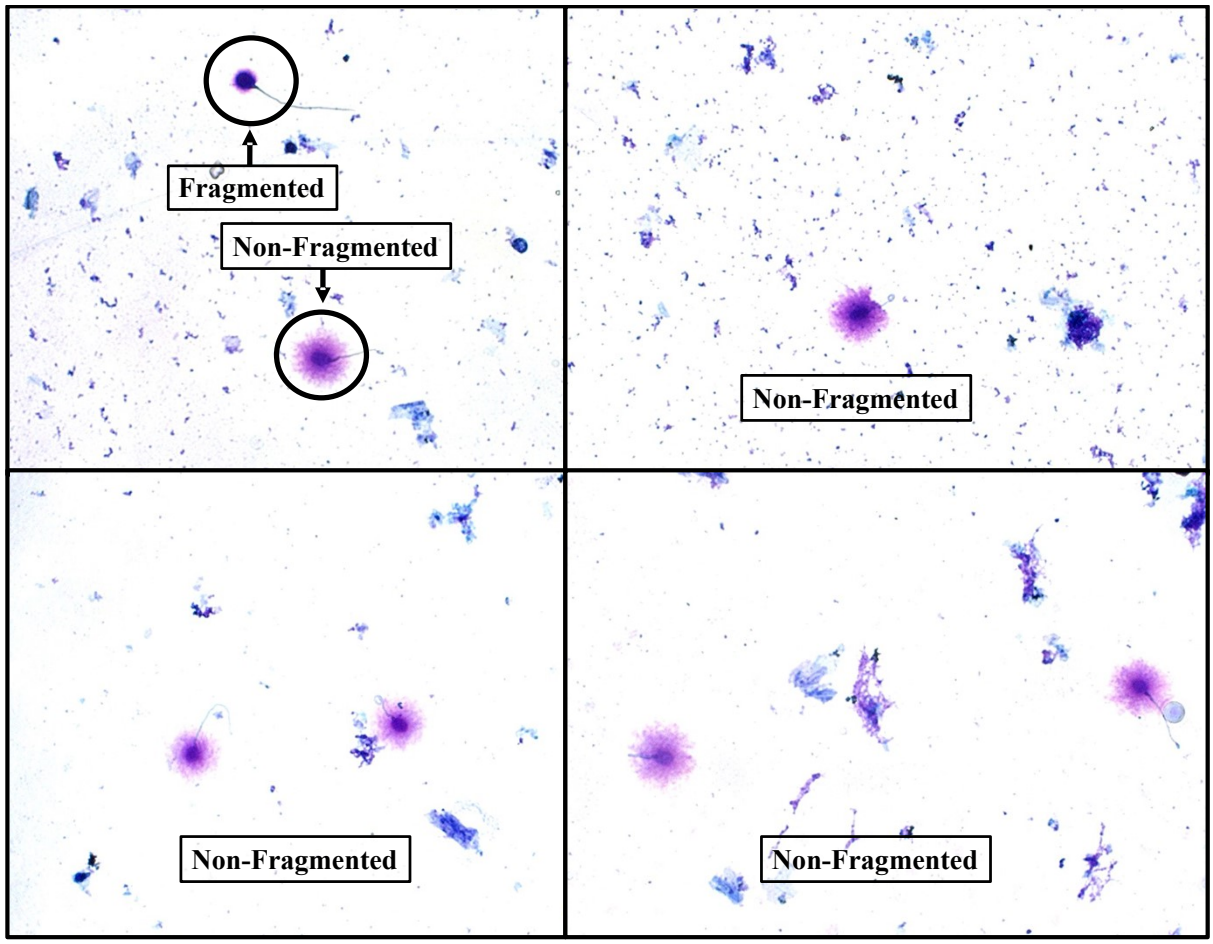

Fig. S3 (C): 40X objective brightfield images of the sperm cells isolated from the collection chamber of the with-flow (0.5 $\mu l/min$) chip settings. Sperm cells showing big and medium halo have non-fragmented DNA. Sperm cells showing no halo have fragmented DNA.

6. Isolation efficiency plot

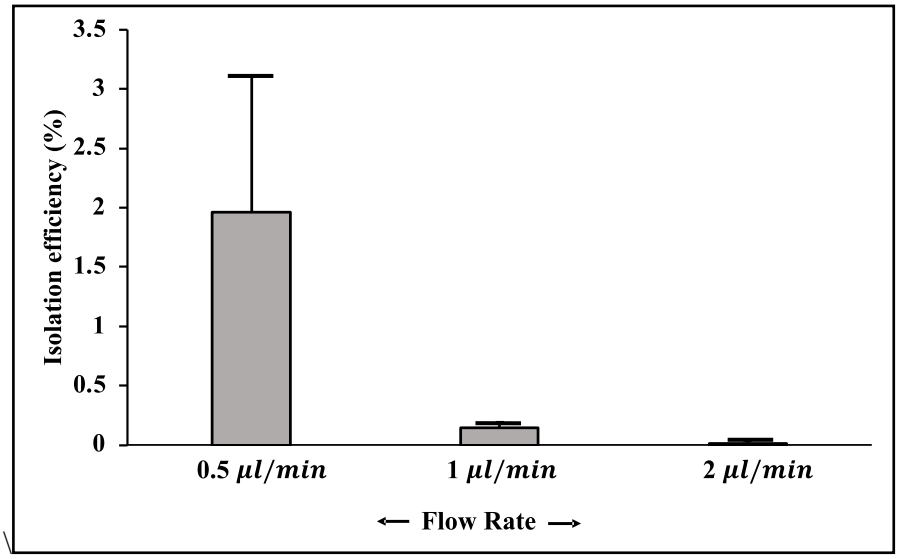

Fig. S4: Isolation efficiency comparison between the different flow rates to examine the optimal flow rate for sperm cell selection on the microfluidic chip.

7. COMSOL results

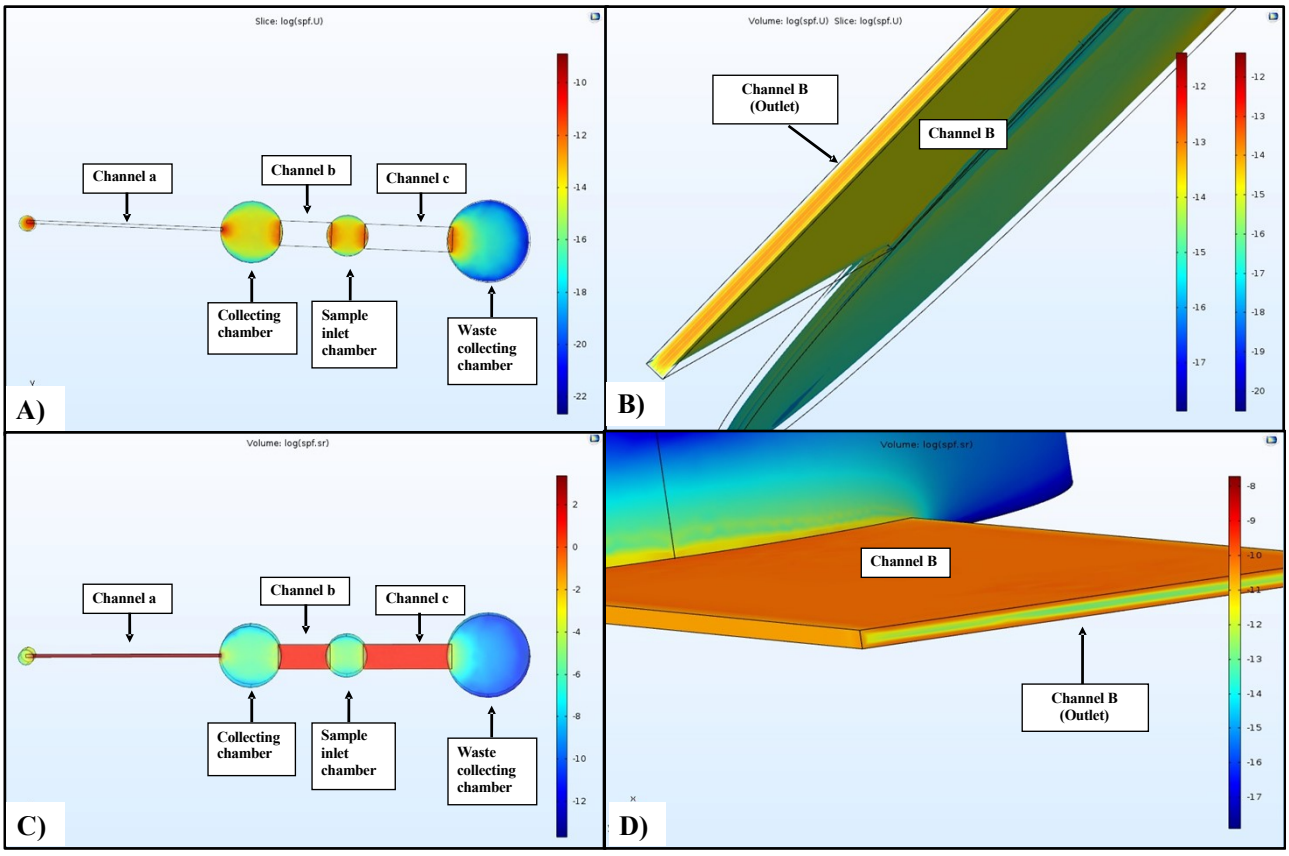

Fig. S5 (A): Slice log velocity magnitude (a.u.) of the collection sample inlet and waste collection chambers. (**B):** the log velocity profile (slice & volume) simulation of the microfluidic chip representing the inside view of channel "b" showing the velocity is higher in the center and lower against the walls. (**C**): volume log shear stress profile (a.u.) of the microfluidic chip. **(D):** volume log shear stress profile of the channel "b" showing shear stress is higher against the walls and lower in the center. In reality, the outlet of channel "b" is connected to the inlet chamber of the chip.

Computational results:

The slice log velocity profile of the microfluidic chip in COMSOL demonstrated that chambers have different velocity sketches. As the volume of the chambers is larger, the velocity of the fluid inside the chambers is very low. However, the velocity at the end and beginning of the channels is higher (**Fig. S5 A**). The log volume and slice velocity profile of channel b (inside view) showed higher velocity in the center than in the walls (**Fig. S5 B**). The results of the volume log shear stress profile of the microfluidic chip revealed high shear stress in the channels and low in the chambers (**Fig. S5 C**). The volume log shear stress profile of channel b (inside view) showed high shear stress against the walls of channel "b" and low in the center (**Fig. S5 D**).

8. References:

1. I. R. Sarbandi, A. Lesani, M. Moghimi Zand and R. Nosrati, *Scientific Reports*, 2021, **11**, 1-8.
2. Y. Yan, H. Liu, B. Zhang and R. Liu, *Micromachines*, 2020, **11**, 793.
3. A. Ataei, A. Lau and W. Asghar, *Microfluidics and Nanofluidics*, 2021, **25**, 1-10.
4. C.-k. Tung, F. Ardon, A. G. Fiore, S. S. Suarez and M. Wu, *Lab on a Chip*, 2014, **14**, 1348-1356.
5. C.-k. Tung, L. Hu, A. G. Fiore, F. Ardon, D. G. Hickman, R. O. Gilbert, S. S. Suarez and M. Wu, *Proceedings of the National Academy of Sciences*, 2015, **112**, 5431-5436.
6. M. Zaferani, S. H. Cheong and A. Abbaspourrad, *Proceedings of the National Academy of Sciences*, 2018, **115**, 8272-8277.
7. K. Rappa, J. Samargia, M. Sher, J. S. Pino, H. F. Rodriguez and W. Asghar, *Microfluidics and Nanofluidics*, 2018, **22**, 1-11.
8. M. Zaferani, G. D. Palermo and A. Abbaspourrad, *Science advances*, 2019, **5**, eaav2111.
9. R. Samuel, N. Miller, O. Badamjav, T. Jenkins, D. Carrell, J. Hotaling and B. K. Gale, *Journal of Micromechanics and Microengineering*, 2018, **28**, 097002.
10. H. Kang, T. An, D. Lee and B. Kim, *Review of Scientific Instruments*, 2019, **90**, 084101.
11. B. Hwang, D. Lee, S.-J. Hwang, J.-H. Baek and B. Kim, *International Journal of Precision Engineering and Manufacturing*, 2019, **20**, 1037-1045.
12. T. M. El-Sherry, M. Elsayed, H. K. Abdelhafez and M. Abdelgawad, *Integrative Biology*, 2014, **6**, 1111-1121.
13. M. A. Abdel-Ghani, T. El-sherry, G. Mahmoud and M. Nagano, *Reproduction in Domestic Animals*, 2020, **55**, 1541-1547.
14. T. El-sherry, M. Abdel-Ghani, N. Abou-Khalil, M. Elsayed and M. Abdelgawad, *Reproduction in Domestic Animals*, 2017, **52**, 781-790.
15. J.-K. Wu, P.-C. Chen, Y.-N. Lin, C.-W. Wang, L.-C. Pan and F.-G. Tseng, *Analyst*, 2017, **142**, 938-944.
16. Y.-A. Chen, Z.-W. Huang, F.-S. Tsai, C.-Y. Chen, C.-M. Lin and A. M. Wo, *Microfluidics and Nanofluidics*, 2011, **10**, 59-67.
17. K. Shirota, F. Yotsumoto, H. Itoh, H. Obama, N. Hidaka, K. Nakajima and S. Miyamoto, *Fertility and sterility*, 2016, **105**, 315-321. e311.
18. T. Chinnasamy, J. L. Kingsley, F. Inci, P. J. Turek, M. P. Rosen, B. Behr, E. Tüzel and U. Demirci, *Advanced Science*, 2018, **5**, 1700531.
19. B. Panigrahi and C.-Y. Chen, *Lab on a Chip*, 2019, **19**, 4033-4042.
20. H.-Y. Huang, P.-W. Huang and D.-J. Yao, *Microsystem Technologies*, 2017, **23**, 305-312.
21. L. Eamer, M. Vollmer, R. Nosrati, M. C. San Gabriel, K. Zeidan, A. Zini and D. Sinton, *Lab on a Chip*, 2016, **16**, 2418-2422.